Activation of periodate by biocarbon-supported multiple modified nanoscale iron for the degradation of bisphenol A in high-temperature aqueous solution.

Jingnan Zhao[1,2,*]; Junwen Chen [2,3,*] ;Qun Wang [2,**]; Renxuan Xiong [2]; Jun Ma[4]

[1] *The IT Electronics Eleventh Design & research Institute Science and Technology Engineering co., LTD.*

[2] *Faculty of Geoscience and Environmental Engineering, Southwest Jiaotong University, Chengdu 610031, P.R. China;*

[3] *School of Chemical Engineering and Advanced Materials, The University of Adelaide, Adelaide, SA 5005, Australia.*

[4] *State Key Laboratory of Urban Water Resource and Environment, Harbin Institute of Technology, Harbin 150090, PR China.*

[*] *These authors have contributed equally to this work.*

** *Corresponding author.*

Tel: +86 18215559048; E-mail: xhlu_swjtu@126.com (Q. Wang);

Table S1: Relevant typical research on the application of modified nanometal catalytic materials in the advanced oxidation processes

Catalytic	Oxidants	Target pollutants	Results	Reference
Zero Valent Iron (ZVI)-Sludge Derive Various catalytic parameters were thoroughly investigated d Biochar (SDBC)（ZVI-SDBC）	persulfate	acid orange (AO7) and landfill leachate	The advantages of ZVI-SDBC included the superior, pH-independent, and sustainable performance as a PS activator, It is of great significance for the treatment of organically polluted wastewater, groundwater, and soil.	Wang et al. (2020)
‘nuclear-shell structure iron-carbon nanocomposite (Fe@CNs)	persulfate	BPA	Fe@CNs, a new and successful attempt for PS to degrade BPA efficiently	Liu et al. (2020)
Fe@N-doped graphene-like carbon	Peroxy-mono sulfate	4-aminobenzoic acid ethyl ester (ABEE) and sulfamethoxazole (SMX)	It has good catalytic properties of peroxymonosulfate， This study provided a new insight to fabricate high-efficiency activation mediator combined metal and N-doped graphene-like carbon from MOFs for advanced oxidation processes.	Liu et al. (2019)
novel nano zero-valent iron anchored yCo3O4 (nZVI/yCo3O4) composites	Peroxy disulfate	tetracycline	the synthesized heterogeneous nZVI/yCo3O4 composites can efficiently active PS at a wide pH range, and further broaden the application of Co-based catalysts in PS activation	Wang et al. (2019)
Granular activated carbon (GAC) supported ZnO catalyst (ZnO-GAC)	persulfate	Acid Orange 7	It has good catalytic properties of persulfate， The reusability of ZnO-GAC was unsatisfactory	Liu et al. (2018)
carbon-encapsulated metal nanoparticles （FeNi@C,Fe@c,Ni@C,Cu@C)	Peroxymonosul-fate	Bisphenol A. carbamazepine etc	metal@C NPsprepared in this study is superior to pristine metal NPs in terms of chemical stability， And better catalytic performance	Yun et al. (2020)
FeOx/MnOy decorated oxidized carbon nanotubes (CNTs-Fe-Mn) composites	Peroxymonos-sulfate	rhodamine B (RhB)	CNTs-Fe-Mn can activate peroxymonosulfate efficiently and also display excellent performance of long-term stability for the degradation of organic pollutants in water.	Tian and Xiao (2020)
Fe-doped BiOCl nanosheets	persulfate	levofloxacin	The catalysts show good catalytic performance and stability， the good feasibility of Fe-doped BiOCl nanosheets which would enhance the utilization of photocatalysts under visible light	Zhong et al. (2020)
Fe0-based nanomaterials（nZVI，S-nZVI,Ni-nZVI,C-nZVI）	sulfite	sulfamethazine	In general, the catalytic effect of the three nano zero-valent iron modified catalysts is generally better than that of bare NZVI	Li et al. (2020)
sulfide-modified nanoscale iron supported by biochar (S-nZVI/BC)	persulfate	ciprofloxacin	Results showed that S-nZVI/BC exhibited excellent performance in removing CIP when combined with PS， S-nZVI/BC is an ideal catalyst for PS activation for antibiotics treatment	Gao et al. (2020)
Iron/copper bimetallic nanoparticles-based sludge biochar (Fe/Cu-SBC)	periodate	diclofenac sodium	The type and number of surface functional groups were found to be increased and the catalytic performance was improved by the modification of Fe/Cu bimetallic nanoparticles。 Therefore, this investigation provides a feasible alternative for the degradation of PPCPs in wastewater.	He et al. (2021)

carbon nanotube supported nanoscale zerovalent copper(nZVC–CNT)	Peroxymonos-sulfate	Congo red	nZVC–CNT were developed to serve as high-performance catalysts, electrode, and filtration media simultaneously,	Wentian et al. (2021)

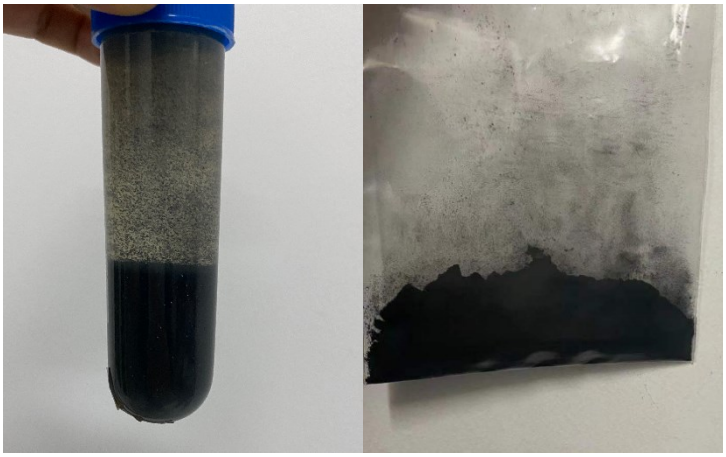

Fig.S1 Diagram of semi-finished and fresh S-(nFe^0-Ni)/BC.

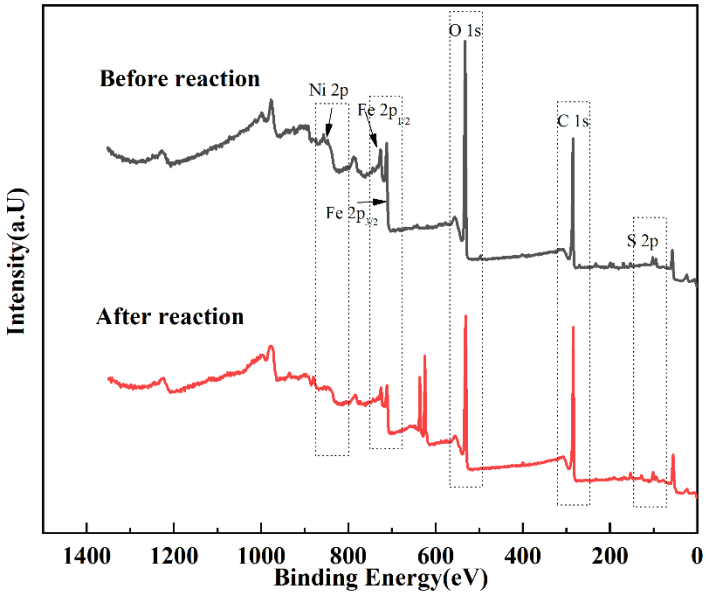

Fig.S2 XPS full scan pattern of S-(nFe^0-Ni)/BC (before and after reaction).

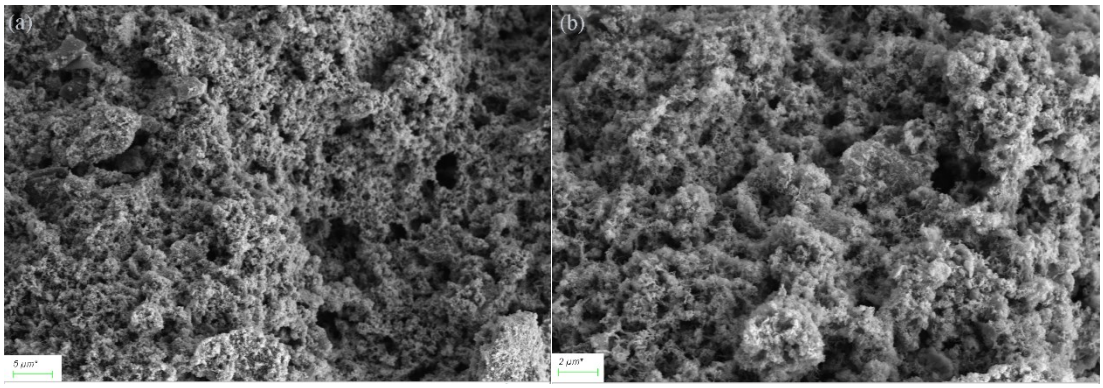

Fig.S3 SEM morphology of S-(nFe^0-Ni)/BC. (a) 4000 times; (b) 10000 times

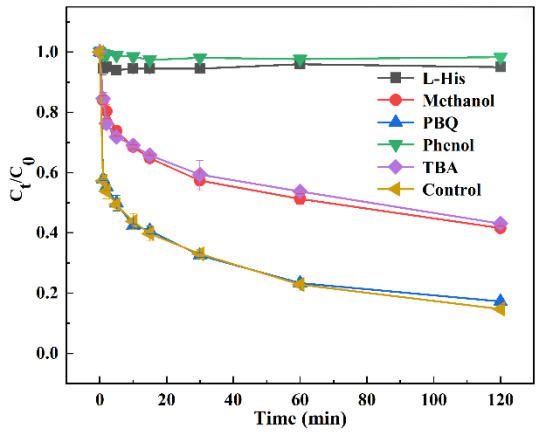

Fig.S4 Effect of different free radical scavengers on the degradation of BPA in high temperature wastewater by S-(nFe^0-Ni)/BC /PI system; [BPA]$_0$:20μM, [PI]$_0$:1mM, S-(nFe^0-Ni)/BC:0.2g/L, Temperature: 65°C, initial pH:4.0; L-His, Methanol, PBQ, Phenol, TBA:10mM.

Effect of dissolved oxygen.

In the presence of oxygen, it mainly affects $O_2^{\bullet-}$, •OH、O(^{3}P)，compared with the standard system, the degradation rate of BPA decreased by 8.4% in the absence of oxygen, indicating that the above oxygen-containing free radicals exist in the system, but they did not play a dominant role in the degradation of BPA. This is consistent with previous research results. In addition, the degradation of BPA was inhibited under oxygen saturation, There may be two reasons for this: (1) when DO was too high, it will inhibit the production of •OH, (2) excessive dissolved oxygen in the water will consume Fe^{2+} as an important active intermediate, thereby affecting the generation of main active species $IO_3^{\bullet}$, directly leading to a decrease in the degradation efficiency of BPA(from 3.2.2). The equation is as follows:

$$O(^3P) + O_2 \rightarrow O_3 \quad (1)$$

$$4Fe^{2+} + O_2 + 4H^+ \rightarrow 4Fe^{3+} + 2H_2O \quad (2)$$

$$IO_4^- + 2Fe^{2+} + 2H_2O \rightarrow IO_3^{\bullet} + 2Fe^{3+} + 2\,O_2^{\bullet-} + 4H^+ \quad (3)$$

$$IO_3^{\bullet} + BPA \rightarrow IO_3^- + products \quad (4)$$

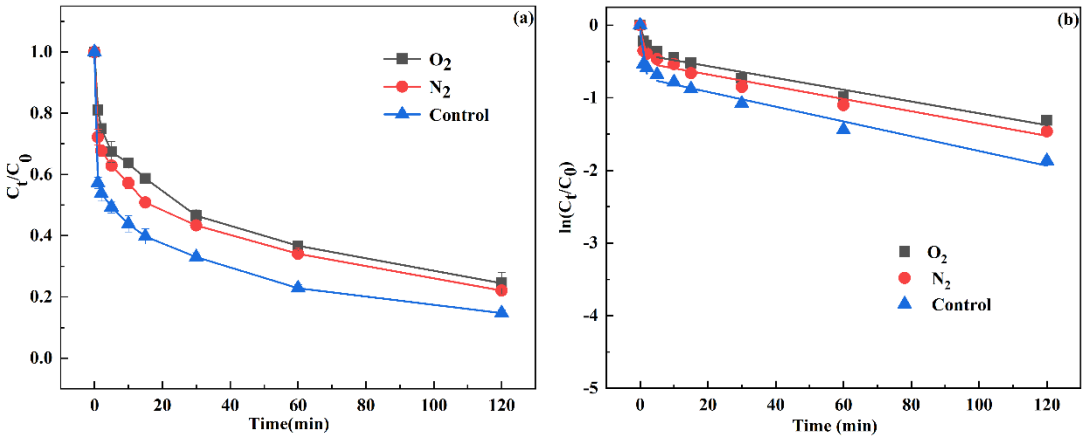

Fig.S5 Efficiency of {S-(nFe^0-Ni)/BC}/PI in degrading BPA in high-temperature wastewater under oxygen saturation and anaerobic conditions; (a) degradation efficiency; (b) pseudo-first-order kinetic fitting; [BPA]$_0$:20μM, [PI]$_0$:1mM, S-(nFe^0-Ni)/BC:0.2g/L, Temperature: 65°C, initial pH:4.0.

Table S2 Kinetic constants of {S-(nFe^0-Ni)/BC}/PI degradation of BPA in high-temperature wastewater under oxygen saturation and anaerobic conditions.

Gas environment (°C)	k_{obs_1}(min^{-1})	R_1^2	k_{obs_2}(min^{-1})	R_2^2
O_2	0.1383	0.8886	0.0081	0.9555
N_2	0.1965	0.8285	0.0085	0.9584
Control	0.2936	0.8158	0.0105	0.9720

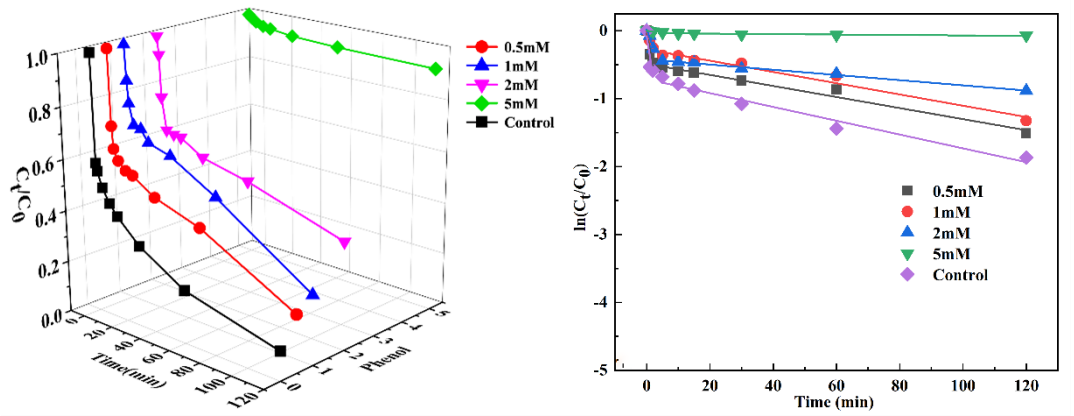

Fig.S6 Efficiency of {S-(nFe^0-Ni)/BC}/PI degradation of BPA in high-temperature wastewater under different concentrations of Phenol addition; [BPA]$_0$:20μM, [PI]$_0$:1mM, S-(nFe^0-Ni)/BC:0.2g/L, Temperature: 65°C, initial pH:4.0; Phenol:0.5,1,2,5mM.

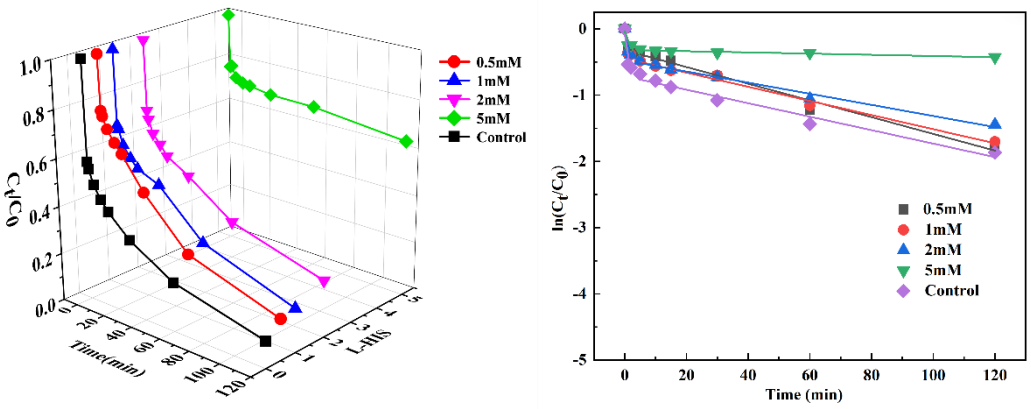

Fig.S7 Efficiency of {S-(nFe^0-Ni)/BC}/PI degradation of BPA in high-temperature wastewater under different concentrations of L-HIS addition; [BPA]$_0$:20μM, [PI]$_0$:1mM, S-(nFe^0-Ni)/BC:0.2g/L, Temperature: 65°C, initial pH:4.0; L-HIS:0.5, 1, 2, 5mM.

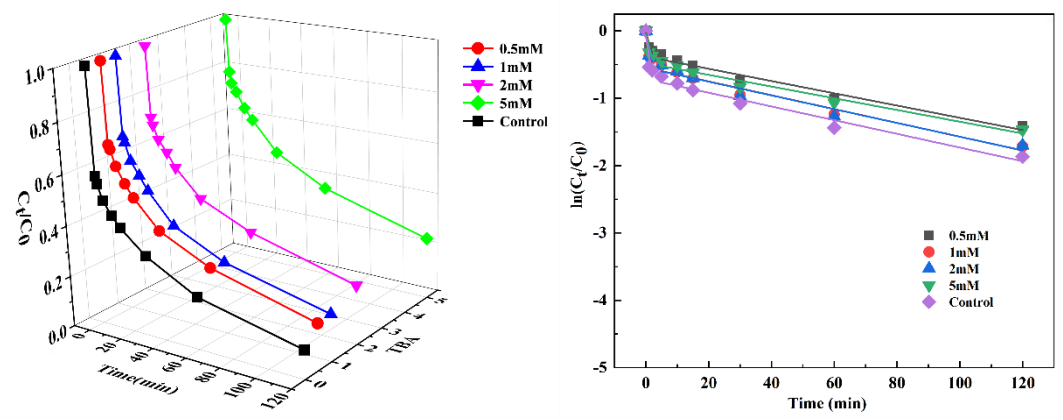

Fig.S8 Efficiency of {S-(nFe^0-Ni)/BC}/PI degradation of BPA in high-temperature wastewater under different concentrations of TBA addition; [BPA]$_0$:20μM, [PI]$_0$:1mM, S-(nFe^0-Ni)/BC:0.2g/L, Temperature: 65°C, initial pH:4.0;TBA:0.5, 1, 2, 5mM.

Table S3 Kinetic constants of {S-(nFe^0-Ni)/BC}/PI degradation of BPA in high-temperature wastewater under different scavengers.

	k_{obs_1}(min^{-1})	R_1^2	k_{obs_2}(min^{-1})	R_2^2
Phenol(0.5mM)	0.2381	0.9362	0.0081	0.9768
Phenol(1mM)	0.1255	0.9920	0.0083	0.9714
Phenol(2mM)	0.1331	0.9354	0.0038	0.9936
Phenol(5mM)	0.0062	0.9997	0.0003	0.7636
L-HIS(0.5mM)	0.1432	0.8229	0.0126	0.9819
L-HIS(1mM)	0.1950	0.7893	0.0107	0.9908
L-HIS(2mM)	0.1972	0.8446	0.0084	0.9866
L-HIS(5mM)	0.1229	0.7332	0.0009	0.9422
TBA(0.5mM)	0.1505	0.8927	0.0091	0.9719
TBA(1mM)	0.2032	0.7960	0.0103	0.9717
TBA(2mM)	0.2003	0.8099	0.0105	0.9608
TBA(5mM)	0.1833	0.8354	0.0087	0.9682
Control	0.2936	0.8159	0.0105	0.9708

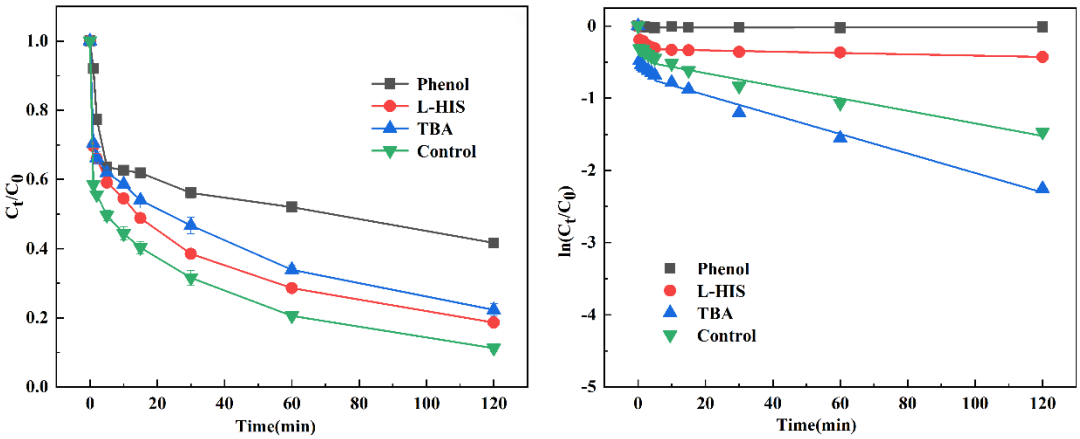

Fig.S9 Efficiency of {S-(nFe^0-Ni)/BC}/PI system for degradation of BPA in high-temperature wastewater under different scavengers for 5-120 minutes; [BPA]$_0$:20μM, [PI]$_0$:1mM, S-(nFe^0-Ni)/BC:0.2g/L, Temperature: 65°C, initial pH:4.0;TBA,L-HIS, Phenol:2mM.

Table S4 Kinetic constants of {S-(nFe^0-Ni)/BC}/PI degradation of BPA in high-temperature wastewater under different scavengers for 5-120min period.

	$k_{obs_2}(min^{-1})$	R_2^2
TBA(2mM)	0.0091	0.9708
L-HIS(2mM)	0.0084	0.9866
Phenol(2mM)	0.0038	0.9936
Control	0.0105	0.9720

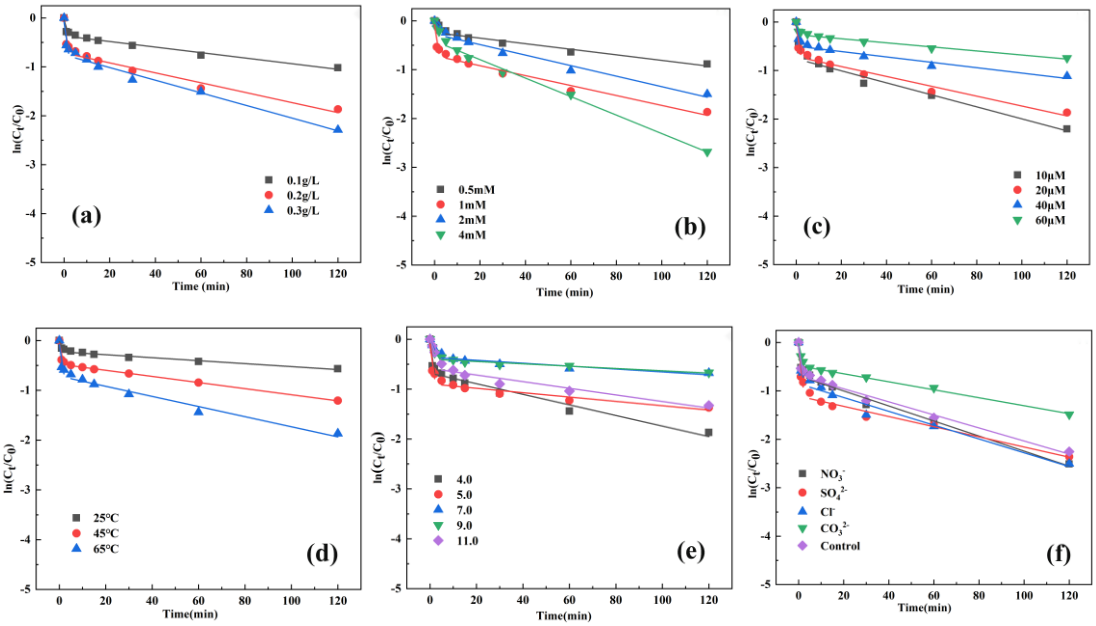

Fig.S10 The degradation pseudo-first-order kinetic of BPA solution by varying (a) the S-(nFe^0-Ni)/BC dosage ([BPA]$_0$:20μM, [PI]$_0$:1mM, Temperature: 65°C, initial pH:4.0); (b) the PI dosage (BPA]$_0$: 20μM, S-(nFe^0-Ni)/BC:0.2g/L, Temperature: 65°C, initial pH:4.0); (c) the BPA dosage ([PI]$_0$:1mM, S-(nFe^0-Ni)/BC:0.2g/L, Temperature: 65°C, initial pH:4.0); (d) catalytic temperature ([BPA]$_0$:20μM, [PI]$_0$:1mM, S-(nFe^0-Ni)/BC:0.2g/L, initial pH:4.0); (e) the initial pH in the {S-(nFe^0-Ni)/BC}/PI system ([BPA]$_0$:20μM, [PI]$_0$:1mM, S-(nFe^0-Ni)/BC:0.2g/L, Temperature: 65°C); (f) effect of different anions on BPA degradation in the {S-(nFe^0-Ni)/BC}/PI system ([BPA]$_0$:20μM, [PI]$_0$:1mM, S-(nFe^0-Ni)/BC:0.2g/L, Temperature: 65°C, initial pH:4.0, NO_3^-, Cl^-, SO_4^{2-}, CO_3^{2-}:5mM).

Table S5 Kinetic constants of {S-(nFe^0-Ni)/BC}/PI degradation of BPA in high temperature wastewater at different dosages of S-(nFe^0-Ni)/BC.

[Dosage] (g/L)	k_{obs_1}(min^{-1})	R_1^2	k_{obs_2}(min^{-1})	R_2^2
0.1	0.1478	0.7890	0.0057	0.9794
0.2	0.2936	0.8159	0.0102	0.9708
0.3	0.3217	0.8461	0.0129	0.9815

Table S6 Kinetic constants of {S-(nFe^0-Ni)/BC}/PI degradation of BPA in high-temperature wastewater at different dosages of PI.

[PI] $_0$(mM)	k_{obs_1}(min^{-1})	R_1^2	k_{obs_2}(min^{-1})	R_2^2
0.5	0.0472	0.9959	0.0057	0.9624
1	0.2936	0.8159	0.0105	0.9708
2	0.0640	0.9993	0.0108	0.9772
4	0.1074	0.9393	0.0190	0.9943

Table S7 Kinetic constants of {S-(nFe^0-Ni)/BC}/PI degradation of BPA in high-temperature wastewater at different dosages of BPA.

[BPA] $_0$(μM)	k_{obs_1}(min^{-1})	R_1^2	k_{obs_2}(min^{-1})	R_2^2
10	0.2866	0.8766	0.0123	0.9769
20	0.2936	0.8159	0.0105	0.9708
40	0.2039	0.8542	0.0056	0.9567
60	0.1029	0.7805	0.0042	0.9820

Table S8 Kinetic constants of {S-(nFe^0-Ni)/BC}/PI degradation of BPA in high-temperature wastewater at different catalytic temperature.

Temperature(°C)	k_{obs_1}(min^{-1})	R_1^2	k_{obs_2}(min^{-1})	R_2^2
25	0.0888	0.8467	0.0030	0.9749
45	0.2156	0.8266	0.0061	0.9992
65	0.2936	0.8158	0.0105	0.9712

Table S9 Kinetic constants of {S-(nFe^0-Ni)/BC}/PI degradation of BPA in high-temperature wastewater at different initial pH.

$[pH]_0$	$k_{obs_1}(min^{-1})$	R_1^2	$k_{obs_2}(min^{-1})$	R_2^2
4	0.2935	0.8159	0.0106	0.9634
5	0.3466	0.8179	0.0044	0.9012
7	0.1032	0.9919	0.0029	0.8480
9	0.1368	0.9941	0.0023	0.9214
11	0.1308	0.9999	0.0066	0.9212

Table S10 Kinetic constants of {S-(nFe^0-Ni)/BC}/PI degradation of BPA in high-temperature wastewater at different anions.

Anion(5mM)	$k_{obs_1}(min^{-1})$	R_1^2	$k_{obs_2}(min^{-1})$	R_2^2
NO_3^-	0.2848	0.8174	0.0155	0.9878
SO_4^{2-}	0.4097	0.8509	0.0081	0.971
Cl^-	0.3135	0.8018	0.0143	0.9643
CO_3^{2-}	0.2001	0.9459	0.0082	0.9964
Control	0.2936	0.8158	0.0105	0.9720

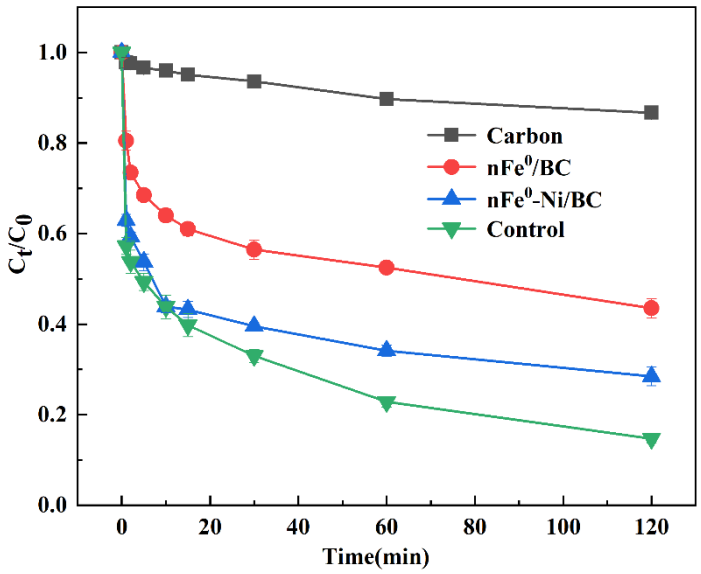

Fig.S11 Comparison of degradation efficiencies under different conditions; catalyst dosage:0.2g/L; $[BPA]_0$:20μM, $[PI]_0$:1mM, Temperature: 65°C, initial pH:4.0.

References

Ao, X., & Liu, W. (2017). Degradation of sulfamethoxazole by medium pressure UV and oxidants: Peroxymonosulfate, persulfate, and hydrogen peroxide. *Chemical Engineering Journal*, *313*, 629-637. https://doi.org/10.1016/j.cej.2016.12.089

Chia, L. H., Tang, X. M., & Weavers, L. K. (2004). Kinetics and mechanism of photoactivated periodate reaction with 4-chlorophenol in acidic solution. *Environmental Science & Technology*, *38*(24), 6875-6880. https://doi.org/10.1021/es049155n

Do, Q. C., Kim, D.-G., & Ko, S.-O. (2017). Nonsacrificial Template Synthesis of Magnetic-Based Yolk-Shell Nanostructures for the Removal of Acetaminophen in Fenton-like Systems. *Acs Applied Materials & Interfaces*, *9*(34), 28508-28518. https://doi.org/10.1021/acsami.7b07658

Gao, J., Han, D., Xu, Y., Liu, Y., & Shang, J. (2020). Persulfate activation by sulfide-modified nanoscale iron supported by biochar (S-nZVI/BC) for degradation of ciprofloxacin. *Separation and Purification Technology*, *235*.

Garcia-Segura, S., Qu, X., Alvarez, P. J. J., Chaplin, B. P., Chen, W., Crittenden, J. C., Feng, Y., Gao, G., He, Z., Hou, C.-H., Hu, X., Jiang, G., Kim, J.-H., Li, J., Li, Q., Ma, J., Ma, J., Nienhauser, A. B., Niu, J., Pan, B., Quan, X., Ronzani, F., Villagran, D., Waite, T. D., Walker, W. S., Wang, C., Wong, M. S., & Westerhoff, P. (2020). Opportunities for nanotechnology to enhance electrochemical treatment of pollutants in potable water and industrial wastewater - a perspective. *Environmental Science-Nano*, *7*(8), 2178-2194. https://doi.org/10.1039/d0en00194e

Glaze, W. H., Kang, J. W., & Chapin, D. H. (1987). The Chemistry of Water Treatment Processes Involving Ozone, Hydrogen Peroxide and Ultraviolet Radiation. *Ozone Science & Engineering*, *9*(4), 335-352.

He, L., Lv, L., Pillai, S. C., Wang, H., Xue, J., Ma, Y., Liu, Y., Chen, Y., Wu, L., Zhang, Z., & Yang, L. (2021). Efficient degradation of diclofenac sodium by periodate activation using Fe/Cu bimetallic modified sewage sludge biochar/UV system. *Science of the Total Environment*, *783*, Article 146974. https://doi.org/10.1016/j.scitotenv.2021.146974

Li, R., Dong, H., Tian, R., Chen, J., & Xie, Q. (2020). Activation of sulfite by different Fe 0 -based nanomaterials for oxidative removal of sulfamethazine in aqueous solution. *Separation and Purification Technology*, *250*.

Liu, C., Liu, L., Tian, X., Wang, Y., Li, R., Zhang, Y., Song, Z., Xu, B., Chu, W., Qi, F., & Ikhlaq, A. (2019). Coupling metal-organic frameworks and g-C3N4 to derive Fe@N-doped graphene-like carbon for peroxymonosulfate activation: Upgrading framework stability and performance. *Applied Catalysis B-Environmental*, *255*, Article 117763. https://doi.org/10.1016/j.apcatb.2019.117763

Liu, F., Yi, P., Wang, X., Gao, H., & Zhang, H. (2018). Degradation of Acid Orange 7 by an ultrasound/ZnO-GAC/persulfate process. *Separation and Purification Technology*, *194*.

Liu, L., Xu, X., Li, Y., Su, R., Li, Q., Zhou, W., Gao, B., & Yue, Q. (2020). One-step

synthesis of "nuclear-shell" structure iron-carbon nanocomposite as a persulfate activator for bisphenol A degradation. *Chemical Engineering Journal*, *382*, Article 122780. https://doi.org/10.1016/j.cej.2019.122780

Qin, W., Fang, G., Wang, Y., & Zhou, D. (2018). Mechanistic understanding of polychlorinated biphenyls degradation by peroxymonosulfate activated with CuFe2O4 nanoparticles: Key role of superoxide radicals. *Chemical Engineering Journal*, *348*, 526-534. https://doi.org/10.1016/j.cej.2018.04.215

Tian, X., & Xiao, L. (2020). FeOx/MnOy modified oxidized carbon nanotubes as peroxymonosulfate activator for organic pollutants degradation. *Journal of Colloid and Interface Science*, *580*, 803-813. https://doi.org/10.1016/j.jcis.2020.07.081

Wang, J., Shen, M., Gong, Q., Wang, X., Cai, J., Wang, S., & Chen, Z. (2020). One-step preparation of ZVI-sludge derived biochar without external source of iron and its application on persulfate activation. *Science of the Total Environment*, *714*, Article 136728. https://doi.org/10.1016/j.scitotenv.2020.136728

Wang, Q., Cao, Y., Zeng, H., Liang, Y., Ma, J., & Lu, X. (2019). Ultrasound-enhanced zero-valent copper activation of persulfate for the degradation of bisphenol AF. *Chemical Engineering Journal*, *378*, Article 122143. https://doi.org/10.1016/j.cej.2019.122143

Wentian, Z., Yanbiao, L., Wen, L., Haodong, J., Fang, L., Chensi, S., Xiaofeng, F., Xiang, L., & Xiaoguang, D. (2021). A novel electrocatalytic filtration system with carbon nanotube supported nanoscale zerovalent copper toward ultrafast oxidation of organic pollutants. *Water research*, *194*.

Yun, E.-T., Park, S.-W., Shin, H. J., Lee, H., Kim, D.-W., & Lee, J. (2020). Peroxymonosulfate activation by carbon-encapsulated metal nanoparticles: Switching the primary reaction route and increasing chemical stability. *Applied Catalysis B: Environmental*, *279*.

Zheng, W., Liu, Y., Liu, W., Ji, H., Li, F., Shen, C., Fang, X., Li, X., & Duan, X. (2021). A novel electrocatalytic filtration system with carbon nanotube supported nanoscale zerovalent copper toward ultrafast oxidation of organic pollutants. *Water research*, *194*, Article 116961. https://doi.org/10.1016/j.watres.2021.116961

Zhong, X., Zhang, K.-X., Wu, D., Ye, X.-Y., Huang, W., & Zhou, B.-X. (2020). Enhanced photocatalytic degradation of levofloxacin by Fe-doped BiOCl nanosheets under LED light irradiation. *Chemical Engineering Journal*, *383*, Article 123148. https://doi.org/10.1016/j.cej.2019.123148

Peng, L. , Duan, X. , Shang, Y. , Gao, B. , & Xu, X. . (2021). Engineered carbon supported single iron atom sites and iron clusters from fe-rich enteromorpha for fenton-like reactions via nonradical pathways. Applied Catalysis B: Environmental, 287, 119963.

Li, X. , Wang, J. , Duan, X. , Li, Y. , & Peng, W. . (2021). Fine-tuning radical/nonradical pathways on graphene by porous engineering and doping strategies. ACS Catalysis, 4848-4861.

Liu, S. , Jing, B. , Nie, C. , Ao, Z. , & An, T. . (2021). Piezoelectric activation of peroxymonosulfate by mos2 nanoflowers for enhanced degradation of aqueous organic pollutants. Environmental science. Nano.

Liu, X. , Xu, B. , Duan, X. , Hao, D. , Wei, W. , & Wang, S. , et al. Facile preparation of hydrophilic in2o3 nanospheres and rods with improved performances for photocatalytic degradation of pfoa. Environmental Science: Nano.